JPn Neuroscience

The Journal of Physiology

J Physiol 591.10 (2013) pp 2667–2686

Basic properties of somatosensory-evoked responses in the dorsal hippocampus of the rat

Elisa Bellistri[1,2], Juan Aguilar[2], Jorge R. Brotons-Mas[1], Guglielmo Foffani[2] and Liset Menendez de la Prida[1]

[1] *Instituto Cajal CSIC, Ave Doctor Arce, 37, Madrid 28012, Spain*
[2] *Hospital Nacional de Parapléjicos, Servicio de Salud de Castilla-La Mancha, Toledo 45071, Spain*

Key points

- We investigate the elementary responses of the hippocampus to somatosensory stimulation (peripheral and lemniscal) in rats given its relevance for episodic memory function.
- We integrate local field potential and multi-unit data from multisite silicon probes, single-unit data from tetrode recordings and membrane potential data from intracellular recordings.
- Somatosensory signals reach the hippocampus mainly from layer II entorhinal cortex to directly discharge dentate gyrus granule cells, while a different predominantly inhibitory process takes place in CA1, further controlling the hippocampal output.
- Hippocampal responses to somatosensory stimuli were dependent on fluctuations in the strength and composition of synaptic inputs due to changes of the ongoing local (hippocampal) and distant (cortical) state.
- Our data reveal a distinct organization of somatosensory-related extra-hippocampal inputs converging onto dentate gyrus and CA1.

Abstract The hippocampus is a pivotal structure for episodic memory function. This ability relies on the possibility of integrating different features of sensory stimuli with the spatio-temporal context in which they occur. While recent studies now suggest that somatosensory information is already processed by the hippocampus, the basic mechanisms still remain unexplored. Here, we used electrical stimulation of the paws, the whisker pad or the medial lemniscus to probe the somatosensory pathway to the hippocampus in the anaesthetized rat, and multisite electrodes, in combination with tetrode and intracellular recordings, to look at the properties of somatosensory hippocampal responses. We found that peripheral and lemniscal stimulation elicited small local field potential responses in the dorsal hippocampus about 35–40 ms post-stimulus. Current source density analysis established the local nature of these responses, revealing associated synaptic sinks that were consistently confined to the molecular layer (ML) of the dentate gyrus (DG), with less regular activation of the CA1 stratum lacunosum moleculare (SLM). A delayed (40–45 ms), potentially active, current source that outlasted the SLM sink was present in about 50% cases around the CA1 pyramidal cell layer. Somatosensory stimulation resulted in multi-unit firing increases in the majority of DG responses (79%), whereas multi-unit firing suppression was observed in the majority of CA1 responses (62%). Tetrode and intracellular recordings of individual cells confirmed different firing modulation in the DG and the CA1 region, and verified the active nature of both the early ML sink and delayed somatic CA1 source. Hippocampal responses to somatosensory stimuli were dependent on fluctuations in the strength and composition of synaptic inputs due to changes of the ongoing local (hippocampal) and distant (cortical) state. We conclude that somatosensory signals reach the hippocampus mainly from layer II entorhinal cortex to directly discharge DG granule cells, while a different

DOI: 10.1113/jphysiol.2013.251892

predominantly inhibitory process takes place in CA1, further controlling the hippocampal output. Therefore, our data reveal a distinct organization of somatosensory-related extra-hippocampal inputs converging onto DG and CA1.

(Resubmitted 18 January 2013; accepted 15 February 2013; first published online 18 February 2013)
Corresponding authors L. M. de la Prida: Instituto Cajal CSIC, Neurobiología-Investigación, Ave Doctor Arce 37, Madrid 28002, Spain. Email: lmprida@cajal.csic.es; G. Foffani: Hospital Nacional de Parapléjicos, Servicio de Salud de Castilla-La Mancha, Toledo 45071, Spain. Email: guglielmo.foffani@drexel.edu

Abbreviations CSD, current source density; DG, dentate gyrus; iPP, ipsilateral perforant pathway; LFP, local field potential; ML, molecular layer; MUA, multi-unit activity; PSTH, peri-stimulus time histogram; SLM, stratum lacunosum moleculare; SP, stratum pyramidale; SR, stratum radiatum; SW, slow-wave.

Introduction

The hippocampus is a critical structure involved in the formation of episodic memories (Eichenbaum, 2004). To this purpose information from the individual attributes of items and events has to be associated to form a meaningful representation of the whole spatio-temporal context. Such a process takes place as a continuous updating of visual, auditory, olfactory and somatosensory information (O'Keefe & Nadle, 1978; Eacott & Norman, 2004). Understanding how sensory information from different modalities reaches the hippocampus is therefore required in order to uncover specific mechanisms of memory function.

Previous studies have examined the effect of sensory and vestibular information entering the hippocampal formation in freely moving animals (Deawyler *et al.* 1981; Brankack & Buzsaki, 1986; Smith, 1997; Vinogradova, 2001). Unit recordings revealed that multimodal responses (visual, auditory and tactile) occur at the single-cell level (Vinogradova *et al.* 1993; Vinogradova, 2001), probably served by projections from the sensory cortices converging onto the parahippocampal region (Burwell & Amaral, 1998). Interestingly, hippocampal cell responses to sensory stimuli of different modalities were found to be strongly modulated by ongoing theta oscillations (Brankack & Buzsaki, 1986; Vinogradova *et al.* 1993; Pereira *et al.* 2007; Tai *et al.* 2012), and in close relationship with the level of arousal (Vinogradova, 2001). Indeed, sensory stimulation *per se* is known to induce type 2 theta oscillations (Sainsbury *et al.* 1987), thus suggesting a complex interaction between hippocampal responses and the cortical and subcortical control of brain state (Vinogradova, 2001; Tai *et al.* 2012).

Amongst the different sensory modalities (visual, auditory, somatosensory, olfactory), the somatosensory system is, together with olfaction, probably the most important system for exploration in rodents. As animals collect information from the environment, they actively use their whiskers and the paws of the four extremities to explore objects and surfaces. Recent work has revealed a hippocampal representation of tactile information occurring in rats while they perform whisker discrimination tasks (Pereira *et al.* 2007; Itskov *et al.* 2011). According to these data, CA1 neurons form a representation of textures and objects that is highly dependent on the context and the vigilance state of the animal. However, basic mechanisms underlying somatosensory processing by the hippocampus still remain unclear. Equally unknown is how somatosensory information integrates into the hippocampus, as a detailed analysis of the extracellular and intracellular neuronal processes is lacking.

Here, we use the urethane-anaesthetized preparation to look at the elementary responses of the hippocampus to somatosensory stimulation in rats, integrating (a) local field potential and multi-unit data from multisite silicon probes, (b) single-unit data from tetrode recordings, and (c) membrane potential data from intracellular recordings. We chose to use the anaesthetized preparation so that we could probe the somatosensory pathway to the hippocampus without the influence of the animal's behaviour and of the spatiotemporal context (Deadwyler *et al.* 1981; Brankack & Buzsaki, 1986; Pereira *et al.* 2007; Itskov *et al.* 2011). Overall, we show that somatosensory signals consistently reach the hippocampus via the perforant pathway which mostly originates from layer II entorhinal neurons, to directly excite granule cells of the dentate gyrus (DG). In contrast, responses in the CA1 output area were more associated with a delayed membrane potential hyperpolarization and firing inhibition that ran in parallel with a local active source of the local field potentials. Our data suggest that this different balance of excitation and inhibition at different strata, together with a tight dependence on both the local (hippocampal) and the distant (cortical) state of ongoing oscillatory activity, are critical to understand the variability and richness of somatosensory-evoked hippocampal responses.

Methods

Ethical approval

In vivo anaesthetized recordings

Adult Wistar rats (250–400 g) were anaesthetized with urethane (1.1–1.5 g kg^{-1}, I.P.) and fastened to the stereotaxic frame. Body temperature was kept constant at 37°C with a heating blanket. The urethane injection took approximately 30 min to induce a stage that fluctuated between III-3 and III-3/4 of anaesthesia (Friedberg *et al.* 1999), as monitored with the reflex responses (pinch withdrawal, corneal, eyelid) and electrocorticographic activity. Small holes of 2.0 mm diameter were drilled in the skull above the hippocampus for extra- and intracellular recordings (AP: −3.9 mm from bregma, ML: 2.8–3.6 mm). In addition, in some experiments we obtained simultaneous cortical recordings using either tungsten electrodes or saline-filled glass pipettes at 1.1–1.5 mm depth (infragranular layers) within the primary somatosensory cortices: forepaw (AP: 0.0–0.5 mm anterior from bregma, ML: 3.5–4.5 mm); hindpaw (AP: –0.5 to −1 mm from bregma, ML: 2–2.5 mm) and whisker (AP: −1 to −2 mm from bregma, ML: 5–6 mm). In some animals, we also performed recordings at the medial lemniscus (AP: −5.0 mm, ML: 1 mm from bregma and depth 7.3 mm) using a bipolar stainless steel electrode (350 μm separation) in bipolar configuration. Two other small holes were drilled to place the CA3 stimulation electrode (AP: −1.2, ML: 2.9, angle 30 deg in the sagittal plane) at the contralateral hemisphere and the ipsilateral perforant pathway stimulation electrode (AP: −7.0, ML: 3.5 mm from bregma). CA3 and perforant pathway stimulation consisted of biphasic square pulses of 0.2 ms duration and amplitudes of 0.1–0.6 mA every 15 s. A subcutaneous Ag/AgCl wire was placed in the neck as a reference electrode. The experimental protocols and procedures met the European guidelines for animal experiments (86/609/EEC) and they were approved by the ethics committees of the participating institutions (Instituto Cajal and Hospital Nacional de Parapléjicos).

Multisite recordings were obtained with linear silicon probe arrays of 16 or 32 sites at 50 or 100 μm vertical spacing (NeuroNexus Tech). They were positioned to record from all strata simultaneously, from the CA1 to the dentate gyrus, as previously described (Ibarz *et al.* 2010). Extracellular signals were preamplified (4× gain) and recorded with a 16- or 32-channel (ch) AC amplifier (Multichannel Systems, models ME16-FAI-μPA-System and USB-ME32-FAI-System, respectively), further amplified by 100, filtered by analog means at 1 Hz to 5 kHz, and sampled at 20 kHz/channel with 12 bit precision. Silicon probes were positioned guided by CA3 and perforant pathway stimulation, together with information from the local field potentials and multi-unit firing. Their lateral and antero-posterior position was later confirmed using the red fluorescent dye 1,1′-dioctadecyl-3,3,3′,3′-tetramethylindocarbocyanine perchlorate (DiI) (Invitrogen) at the end of the experiments by retracting and reinserting the probe.

Single-unit recordings were obtained using commercially available tetrodes (Thomas Recording). Tetrodes were advanced through the different hippocampal strata and guided by CA3 and perforant pathway stimulation. Intracellular recordings were obtained with sharp electrodes and using a dual intracellular amplifier (Axoclamp 2B, Molecular Devices). Sharp electrodes were made from capillary tubes with intraluminal glass fibres (borosilicate, o.d. 1.5 mm, i.d. 0.86 mm; Harvard Apparatus) pulled with a Brown–Flaming horizontal puller (Model P-97; Sutter Instrument Co.), and filled with 2.5 M potassium acetate (electrode resistances: 40–100 MΩ). These recordings were included only if membrane potentials were more negative than −55 mV and action potentials larger than 50 mV were detected. Tetrode and intracellular data were continuously acquired at 20 kHz (CED1401 and Digidata 1440, respectively) together with at least one extracellular channel. For both tetrode and intracellular recordings, the cisterna magna was opened and the cerebrospinal fluid was drained to decrease pulsation of the brain and favour stability.

Somatosensory stimulation

Somatosensory stimulation was delivered by inserting stainless steel needles in the wrist of the paws and in the whisker pad. Stimulation consisted of biphasic electrical pulses of 1 ms duration. In preliminary experiments we confirmed consistent responses at the primary somatosensory cortex occurring at about 4–6 mA intensity. All responses correspond to averages of 100 individual stimuli applied at a frequency from 0.5 to 0.1 Hz. Such a peripheral stimulation can activate both the leminiscal pathway, which primarily conveys faster tactile and proprioceptive information, and the non-lemniscal pathway, which primarily conveys slower pain and temperature information (Khanna & Sinclair, 1992; Lilja *et al.* 2006; Yague *et al.* 2011). The rationale for using high-intensity electrical pulses instead of more naturalistic light tactile stimuli was twofold: (1) to maximize somatosensory inputs into the hippocampus, as we expected hippocampal responses to be very small, and (2) to minimize variability related to receptive field specificity. In order to verify that the hippocampal responses described in our experiment could be relevant for tactile/proprioceptive processing, in a set of rats we also delivered electrical stimuli (0.3–0.6 mA, 0.2 ms) directly to the medial lemniscus using a bipolar electrode. The position of the lemniscal electrode was confirmed by

bipolar recording of high-frequency responses to whisker pad stimulation. Throughout the paper, we use the term 'stimulation session' to refer to the 100 stimuli delivered to a single stimulation site (hindpaw, forepaw or whiskers) in an individual animal. Different stimulation sessions within animals always corresponded to different stimulation sites. Data from different sessions showed no correlation and therefore different sessions from the same animal were treated as independent.

Single-unit isolation and sorting

For spike sorting, signals were high-pass filtered >360 Hz using FIR-type digital filters and exported to Offline Sorter (OFS, Plexon Inc.). Continuous data were then thresholded at 4–5 standard deviations. Recording epochs exceeding this value were stored obtaining spike waveforms of 1.4 ms duration (0.4 ms pre-threshold and 1 ms post threshold) for each of the four channels of the tetrode. Units were sorted using a combination of an automatic clustering algorithm (K-means or KlustaKwik) and manual refinement using OFS. Multiple approaches were used to optimize unit isolation, including principal components analysis of the spike amplitude, the slide amplitude (the waveform amplitude at a particular time) and other waveform parameters such as interval between the peak and the trough. Abnormal spike waveforms were systematically discarded from the clusters. Both the autocorrelogram and the cross-correlogram between units were carefully inspected for contamination of the refractory period (2 ms), central bins asymmetries, abnormal interactions and other possible artifacts. Cells with low firing rate (less than 100 spikes detected per stimulation session) were not sorted and were included in the multi-unit pool. We used MANOVA and statistics on pairwise comparisons to check for significant cluster separation (Hill *et al.* 2011).

Several waveform parameters were used for cell type classification (Csicsvari *et al.* 1999; Sirota *et al.* 2008), including: (a) the trough-to-peak duration, (b) an asymmetry index calculated from the relative amplitude of the positive peaks that flank the action potential, as described in Sirota *et al.* 2008, (c) background firing rate histogram and (d) the first moment of the autocorrelogram. CA1 pyramidal cells often fire complex-spike bursts of 3–5 action potentials (Ranck, 1973) yielding a characteristic autocorrelogram, which together with other waveform features further helps to separate CA1 principal cells from interneurons. For granule cells, however, separation criteria are not straightforward and we mainly relied on the asymmetry index, trough-to-peak duration and the modulation (theta, gamma) of the background firing rate histogram. A number of sorted units (86/258) remained unclassified.

Data analysis

Local field potentials, unit activity and waveforms were all analysed by routines written in Matlab (The Mathworks, USA). Intracellular data were also analysed using tools from Spike 2 (CED, Cambridge) and Clampfit (Molecular devices).

One-dimensional current source density (CSD) profiles (Freeman & Nicholson, 1975) were calculated using the second spatial derivative of local field potentials. For visualization purposes only, raw CSD were subsequently smoothed using the function *spline* from Matlab. Data was represented as averages of up to 100 individual events. Offset differences were corrected before recordings started. Small impedance differences between sites were responsible for the typical stripes detected in the background CSD. These amplitude inhomogeneities were clearly separated from the evoked CSD response, which is associated with local field potential events. In order to further control for potential CSD artifacts due to poor signal-to-noise ratio we adopted two approaches: (a) raw CSD signals at latencies comparable to local field potential peaks were statistically compared against the 100 ms pre-stimulus baseline CSD to define a detection threshold (usually $>5 \times$ standard deviation (SD)); (b) we used blind source separation of local field potentials with independent component analysis (Makarov *et al.* 2010) to compare somatosensory-evoked CSD generators with those from known laminar responses after Schaffer and perforant path stimulation. This analysis allowed us to validate raw CSD signals at any given stratum. Recording from probes having defective sites were all excluded. Tissue conductivity was considered isotropic and an arbitrary value of 1 was assigned to express CSD signals as millivolts per square millimetre.

Multi-unit activity (MUA) was extracted from the 16-ch silicon probes by high-pass FIR filtering (>300 Hz) local field potential signals from the sites located at the stratum pyramidale of the CA1 region and the granular layer of the DG. A threshold of >5 SD was used to detect non-sorted individual spikes and detection was further supervised to exclude artifact and/or noise contribution. Peri-stimulus time histograms (PSTHs) were obtained by binning (5 ms) MUA spike data and single-unit data. Mean PSTHs of pooled units from tetrodes in a given category were binned at 20 ms for illustration purposes. We used unpaired *t* tests ($P < 0.05$) to evaluate whether the PSTH response in the first 100 ms after stimulation (excluding any stimulus artifact) was significantly different from the baseline firing occurring in the last 100 ms before the stimulation. We tested different windows lengths (50, 75, 100, 125 ms) for statistical purposes and found a 100 ms window to better capture statistical differences, given the typical latencies of hippocampal responses. Using the two post-stimulus and pre-stimulus 100 ms windows, we

defined a PSTH ratio (post-stimulus/pre-stimulus) to look for firing increases (ratio > 1) or decreases (ratio < 1) caused after somatosensory stimulation. PSTH ratios were used to statistically evaluate individual and mean neuronal responses. Data from different stimulation sessions were treated as independent samples for statistical purposes when analysing the full dataset.

For evaluating intracellular responses, stimulus-triggered membrane potentials from individual cells were averaged using 15–25 stimuli. From this, we estimated the peak amplitude and latency of the mean membrane potential response in a window of 150 ms post-stimulus, and the mean ± SD of baseline membrane potential fluctuations (in a window of 100 ms pre-stimulus). Only cells exhibiting membrane potential responses (both depolarizing and hyperpolarizing) larger than 2.5 SD were considered to be responding neurons. All responses were visually verified. CA1 and DG neurons were then grouped in different categories according to their response (depolarization and hyperpolarization). A grand average of the mean membrane potential response was calculated pooling cells in a given category.

To study the state dependence of hippocampal somatosensory responses, the analyses on local field potential and CSD responses were repeated after separating trials into theta and non-theta (slow oscillations + large-irregular activities (LIA)), depending on the hippocampal state immediately preceding each stimulus (pre-stimulation windows of 1500 ms). To study the cortical modulation of hippocampal responses, cortical recordings were band-pass filtered at 300–3000 Hz to isolate MUA, rectified, smoothed and down-sampled at 5 Hz. This processed signal correlates well with membrane potential fluctuations and clearly identifies cortical up and down states (Hasenstaub *et al.* 2007; Aguilar *et al.* 2010). Simultaneous hippocampal tetrode recordings were smoothed and down-sampled at 5 kHz. Spectral analysis of cortical and hippocampal recordings was performed using the Thomson multitaper method in non-overlapping windows of 10 s after mean detrending. The cortical state was classified as slow-wave or activated based on the integral of the power spectrum. To classify the hippocampal state as theta or non-theta we (a) determined the peak of the spectrum, (b) estimated the frequency of the spectral peak and (c) determine whether the frequency peak was greater or lower than 3.5 Hz. Note that during non-theta states the frequency peak is <1 Hz, and the hippocampal state is therefore correctly classified as non-theta. To study phase relationship with the cortical up state, stimuli were visually classified as occurring in an active phase (UP state) or silent phase (DOWN state) of the cortical slow-wave activity based on the cortical MUA.

Data in text and figures are given as mean ± standard deviation. Differences between stimulation sessions were analysed using ANOVA for independent samples, when the full dataset was considered. Comparisons across sessions within animals (i.e. forepaw *vs.* hindpaw *vs.* whisker stimuli) were analysed using ANOVA for dependent samples. *Post hoc t* tests were used to examine differences between means. Correlations were calculated using the Pearson coefficient. The probability that the percentages of significant MUA or single-cell responses could be due to chance (5%) was evaluated using the binomial distribution. All results were considered significant at $P < 0.05$.

Results

Hippocampal local field potential responses to somatosensory stimulation

Eighteen urethane-anaesthetized rats were examined for responses to somatosensory stimulation using linear silicon probe arrays of 16 channels placed in the dorsal hippocampus (Fig. 1*A*). Electrical stimuli were delivered either at the contralateral hindpaw, forepaw, or to the whisker pad in 33 stimulation sessions. The arrays were advanced in the dorso-ventral axis to target hippocampal strata from the stratum oriens (SO) of the CA1 to the hilus of the DG guided by stimulation of the contra-lateral CA3 region and of the ipsilateral perforant pathway (Fig. 1*B*), and from information on the laminar profile of theta, multi-unit and ripple activity. We chose to focus on the DG and the CA1 regions not only because they host the major cortical input streams converging onto the hippocampus, but also because they represent the main input and output regions.

Stimulation of either the forepaw (FP, Fig. 1*Ca*), the hindpaw (HP, Fig. 1*Cb*) or the whisker pad (WH, Fig. 1*Cc*) elicited small local field potential deflections in the order of tens of microvolts at peak latencies of 20–75 ms (FP latency: 37.1 ± 8.4 ms, $n = 9$; HP latency: 46.1 ± 10.1 ms, $n = 17$; WH latency: 31.8 ± 7.8 ms, $n = 7$). As expected from their small amplitude, individual responses were variable from trial to trial, but they were clearly seen after averaging (Fig. 1*C*, averages from 100 stimulation pulses).

In order to look at the current generators of local field potentials and to further exclude volume-conducted effects we performed a current source density analysis (CSD) (Freeman & Nicholson, 1975). We analysed data from 28 stimulation sessions meeting methodological requirements for CSD analysis (see Methods). CSD responses (colour maps) revealed the existence of associated current sinks typically spanning around the hippocampal fissure at the stratum lacunosum moleculare (SLM) of CA1 and the molecular layer (ML) of the DG (Fig. 1*Ca–c*, sinks are blue). These sinks correspond with the positive charge inflow of synaptic currents that traverse neuronal membranes at the distal dendrites of CA1 pyramidal cells and of DG granule cells, respectively.

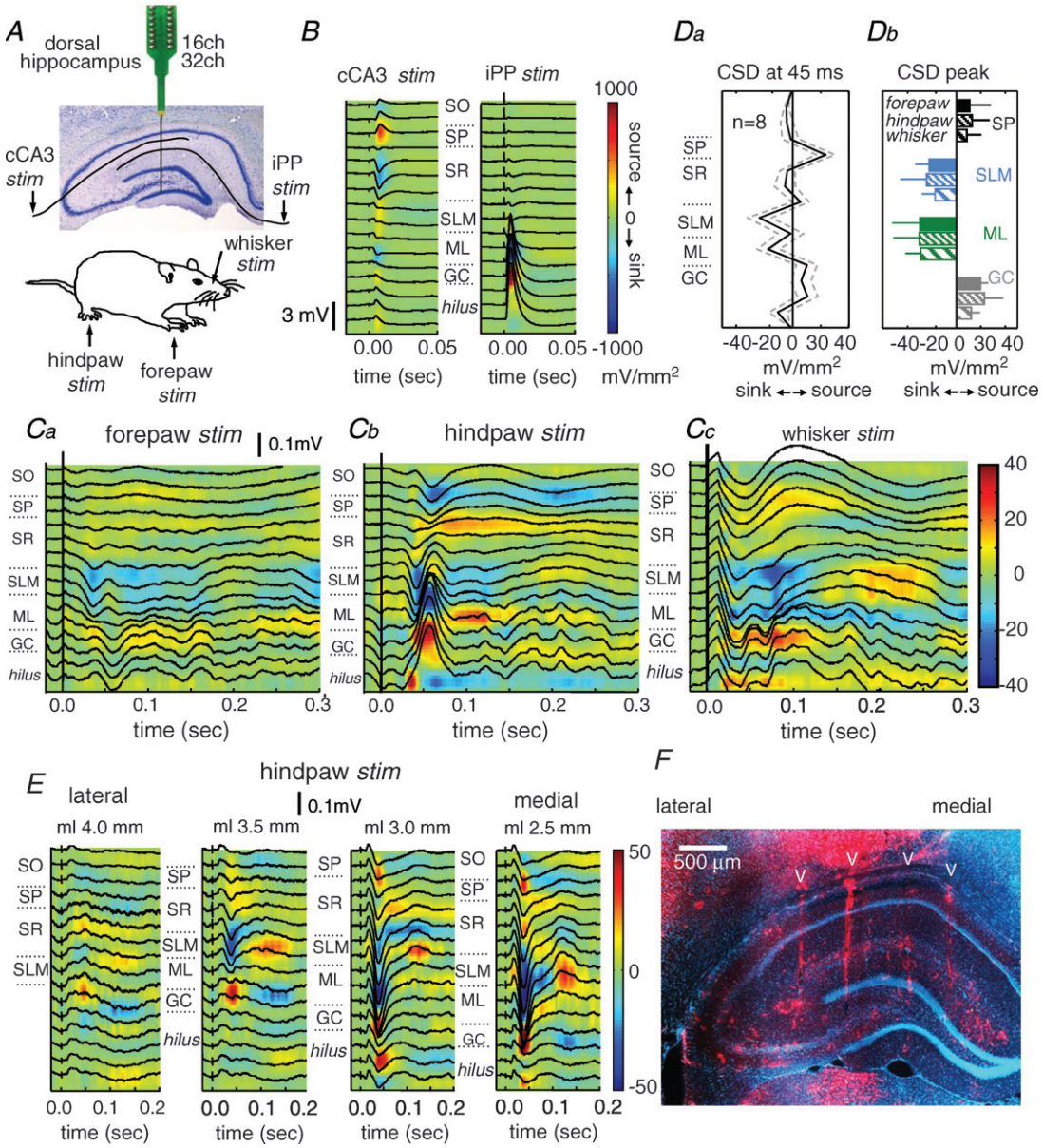

Figure 1. Hippocampal responses to somatosensory stimulation in the urethane-anaesthetized rat
A, multi-site (16 or 32 channel) silicon probes were used to record from the dorsal hippocampus of anaesthetized rats submitted to stimulation of either the contralateral forepaw, hindpaw or the whisker pad. Stimulation of the contralateral CA3 region (cCA3) and the ipsilateral perforant pathway (iPP) were used for localization purposes. *B*, local field potentials and current source density (CSD) maps (underlying colour maps) of the hippocampal responses to cCA3 and iPP facilitated the localization of hippocampal strata. Mean responses from 10 stimuli in one representative rat. Current sources are represented in red while current sinks are blue. SO, stratum oriens, SP, stratum pyramidale, SR, stratum radiatum, SLM, stratum lacunosum molecular, ML, molecular layer, GC, granule cell layer. *C*, mean local field potentials and CSD maps of the hippocampal responses recorded in one rat to stimulation of the forepaw (*Ca*), hindpaw (*Cb*) and the whisker pad (*Cc*). Means obtained by averaging responses to 100 individual stimuli. *Da*, average CSD depth profile at 45 ms. Data from $n = 8$ stimulation sessions with similar spatial sampling. *Db*, mean CSD responses recorded at different hippocampal strata after somatosensory stimulation of the forepaw (FP, dark), hindpaw (HP, thin dashed) and the whisker pad (WH, thick dashed). Means obtained from different stimulation sessions: $n = 14$ SP (black; 3 FP, 7 HP, 4 WH), $n = 15$ SLM (blue; 3 FP, 8 HP, 4 WH), $n = 28$ ML (green; 10 FP, 11 HP, 7 WH) and $n = 28$ GC (grey; same numbers as ML). *E*, mediolateral recordings obtained by parallel insertion of two 16-channel silicon shanks separated by 500 μm. *F*, the fluorescent dye DiI (red) was applied to the probe at the end of experiments for localization purposes. Cell nuclei were stained with bisbenzimide (blue).

They anatomically correspond to the input from the entorhinal cortex into the hippocampus through the temporoammonic (from layer III to SLM) and perforant (from layer II to ML) pathways (Witter *et al.* 2000; Witter, 2007).

The sink at the molecular layer of the DG was consistently present ($n = 28$ of 28 stimulation sessions) and mirrored by a source in the granular cell layer, which contains the somata of granular cells (Fig. 1*Ca–c*). The latency to peak was virtually identical for the DG dendritic sink (38.2 ± 14.9 ms) and for the DG somatic source (38.5 ± 14.6 ms) (paired t test: $P = 0.1184$), suggesting that the DG somatic source most likely represents a passive return current due to somatosensory-evoked activation of granule cells. Sinks at the SLM were less consistently found ($n = 15$ of 28 sessions), as defined by statistical criteria using baseline information. The probability of observing SLM sinks was similar for stimulation of the forepaw, hindpaw and the whisker pad. Often ($n = 14$ of 28 sessions), a current source (red) was detected around the stratum pyramidale (SP) of the CA1 region (Fig. 1*Cc*), sometimes invading the stratum radiatum (SR) (Fig. 1*Cb*). The latency to peak was significantly shorter for the SLM dendritic sink (37.5 ± 15.4 ms) than for the somatic source (45.4 ± 20.7 ms) (paired t test: $P = 0.0002$). In some cases (Fig. 1*Cb*), the somatic source appeared to have an early component that accompanied the SLM sink. However, the longer dynamics of the CA1 somatic source typically outlasting the SLM sink, suggests that the later component of the source cannot simply represent a passive return current, but more likely reflects a complex active process, possibly inhibitory.

The mean profile of sinks and sources at 45 ms clearly showed the presence of all these CSD components (Fig. 1*Da*, data from $n = 8$ sessions from 4 rats with similar spatial sampling). Interestingly, we typically found no clear sink at SR, which contains the excitatory inputs from CA3 (Fig. 1*Ca–c* and *Da*), suggesting that CA3 neuronal firing was unlikely to contribute to the CA1 somatosensory responses in our experimental conditions. Peak CSD responses to somatosensory stimuli of the different limbs and whisker pad were similar in the full dataset (Fig. 1*Db*). Comparisons across stimulation sessions (i.e. forepaw *vs.* hindpaw *vs.* whisker stimuli) within animals ($n = 7$ rats) showed no clear statistical effects of stimulation site on CSD magnitude for the ML sink ($F_{(2,4)} = 0.43$, $P = 0.6601$). Across session data regarding the SLM sink and SP source were only available in $n = 3$ rats preventing analysis of variance.

In eight stimulation sessions from two rats, we also looked at the lateral-to-medial topographic organization of the hippocampal response by using several parallel penetrations with two arrays of 16 channels separated by 500 μm (Fig. 1*E* and *F*). We found the larger sinks to occur around the fissure at the distal part of CA1, typically between 3 mm to about 2.5 mm from the midline (considering the coronal plane at 3.9 mm posterior to bregma). Interestingly, multi-unit responses at the granule cell layer were also larger at these coordinates, further discarding possible bias caused by tangential currents from curving parts at the hippocampal fissure. This is consistent with a different proximo-distal representation of entorhinal inputs arriving into the hippocampus (Witter *et al.* 2000; Witter, 2007), and might suggest that somatosensory information potentially originates from the lateral entorhinal cortex.

Similar hippocampal responses to lemniscal stimulation

High-intensity peripheral stimulation can activate both the lemniscal pathway, which conveys tactile and proprioceptive signals, and the non-lemniscal pathway, which conveys slower pain and temperature signals (Lilja *et al.* 2006; Yague *et al.* 2011). In order to verify that the previously described hippocampal responses could be relevant for tactile/proprioceptive processing, we performed a set of experiments to compare hippocampal responses to peripheral somatosensory stimulation and medial lemniscal stimulation. To this purpose, we monitored neuronal responses at different steps of the synaptic pathway.

We first checked synaptic latencies to whisker stimulation while recording from the medial lemniscus ($n = 14$ stimulation sessions from 11 rats), the S1 barrel cortex ($n = 9$ sessions from 6 rats) and the CA1 or DG cellular layer of the hippocampus ($n = 9$ sessions from 7 rats). Dual recordings were obtained from two of these regions simultaneously in 13 rats (16 sessions). Triple recordings (Fig. 2*A*) were obtained from two rats (2 sessions). Peaks of evoked local field potentials after whisker stimuli were recorded at latencies of 4.64 ± 5.17 ms at the medial lemniscus, 9.83 ± 3.74 ms in the barrel cortex and 27.97 ± 8.13 ms in CA1 (Fig. 2*B*). We then compared peak latencies of evoked potentials recorded at the S1 barrel cortex (Fig. 2*Ca*) and the hippocampus (Fig. 2*Cb*) in whisker *vs.* lemniscal stimulation in an additional set of experiments. Peak latencies in the barrel cortex dropped to 4.77 ± 1.60 ms ($n = 6$ sessions from 6 rats) in response to lemniscal stimulation, being statistically different when compared with direct stimulation of the whisker pad in the same animals (paired t test, $P < 0.01$; Fig. 2*D*). Similarly, in the hippocampus peak latency to medial lemniscus stimulation dropped to 20.11 ± 0.88 ms ($n = 9$ sessions from 9 rats) when compared to stimulation of the whisker pad ($P = 0.0297$, paired t test) (Fig. 2*D*).

We then performed multi-channel recordings to compare CSD profiles in whisker *versus* lemniscal stimulation using 16-ch probes with 50 μm spacing

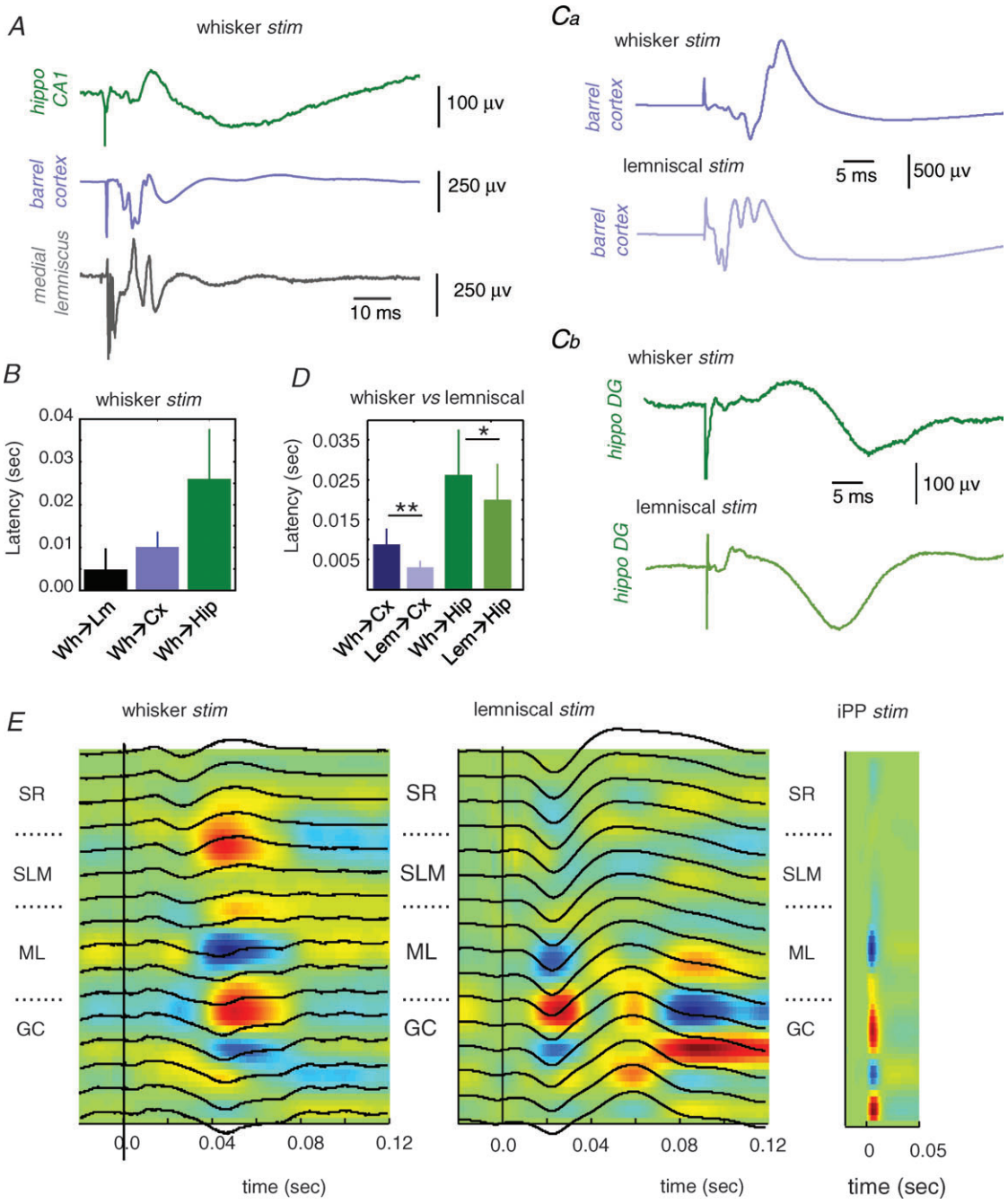

Figure 2. Comparison between whisker and lemniscal stimulation
A, representative example of field potential responses to whisker pad stimulation at different steps of the somatosensory pathway and the hippocampus. *B*, average latency response to whisker pad stimulation (Wh) as recorded in the medial lemniscus (Lm, $n = 14$ stimulation sessions), S1 barrel cortex (Cx, $n = 9$) and the hippocampus (Hip, $n = 9$). *Ca* and *b*, comparison between whisker and lemniscal stimulation in the same animal while recording in the barrel cortex (*Ca*) and the hippocampal DG region (*Cb*). *D*, average latency of the response peak in the barrel cortex ($n = 6$ sessions) and the hippocampus ($n = 9$ sessions) to whisker and lemniscal stimulation. $^*P < 0.05$; $^{**}P < 0.01$. *E*, local field potential (black traces) and CSD responses (underlying colour map) to whisker pad (left), lemniscal (middle) and ipsilateral perforant path (iPP, right) stimulation. Data from 16-channel probes at 50 μm spacing. Sinks are blue; sources are red. Note correspondence between sinks recorded at the molecular layer (ML) for all stimulation sites. SR, stratum radiatum; SLM, stratum lacunosum moleculare; GC, granule cell layer.

around the hippocampal fissure ($n = 6$ sessions/5 rats). We found coincidence of hippocampal sinks at ML when whisker pad stimulation was compared with lemniscal stimulation in the same animals (Fig. 2*E*, ipsilateral perforant pathway (iPP) stimulation was used for localization purposes). Sinks at the SLM were variably encountered in this set of experiments, as previously discussed. Latency of ML CSD responses to lemniscal stimulation were in line with local field potential data (21 ± 6.8 ms). In summary, these data are consistent with a propagation of somatosensory signals into the hippocampus via the medial lemniscal pathway.

Distinct patterns of multi-unit somatosensory responses in CA1 and DG

In order to understand the relationship between synaptic sinks/sources and cellular firing, we further analysed hippocampal cellular responses to peripheral stimuli by extracting multi-unit activity (MUA) from the same silicon probe arrays used in Fig. 1. Peri-stimulus time histograms (PSTHs) were obtained from those electrodes situated at the SP of CA1 and at the granular layer of the DG ($n = 33$ stimulation sessions from 18 rats). Individual PSTH responses in a given session were classified as firing increases, suppression or no changes depending on statistical criteria using baseline information (see Methods). A mean population PSTH was calculated pooling data from different sessions in each category.

Consistent with the small response amplitudes shown in local field potentials, we found statistically significant MUA modulation only in about 48–57% of stimulation sessions for the CA1 region (16 of 33 sessions, binomial $P < 0.0001$) and the DG (19 of 33 sessions, binomial $P < 0.0001$). Remarkably, in the CA1 region there was a predominant MUA suppression in most of the 16 stimulation sessions showing clear PSTH modulation (62%, 10 of 16; Fig. 3*A versus C*). On the contrary, in DG the predominant MUA response was associated with firing increases (79%, 15 of 19; Fig. 3*D*) while firing suppression was seen in only 4 out of the 19 responding cases (Fig. 3*F*).

We next looked at the relationship between the PSTH ratio and the corresponding sinks and sources recorded within the same session to further understand the causes of response differences. To this purpose, we selected those sessions where clear sinks were detected in ML of the DG (28/28) and in SLM of CA1 (15/28). We also included those sessions with clear sources localized around the pyramidal layer of CA1 (14/28). Despite the caveat that extracellular conductances are not necessarily comparable in different sessions/animals, the repeatability of the experimental protocol was high enough to allow us to find significant correlations between CSD and PSTH responses. Specifically, we found correlation between the

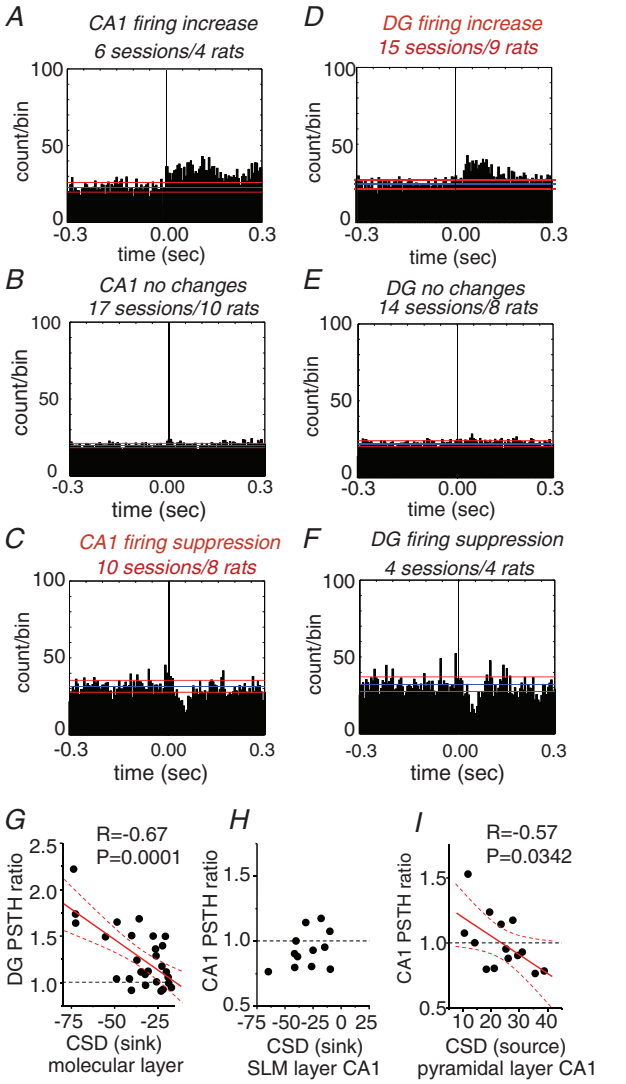

Figure 3. Hippocampal multi-unit activity (MUA) responses to somatosensory stimulation
All histograms represent cumulative data. *A*, MUA recordings obtained from the stratum pyramidale of the CA1 region in 6 stimulation sessions from 4 rats exhibited significant firing increase after somatosensory stimulation. The blue and red lines mark the mean and standard deviation of the baseline firing rate, respectively. *B*, no statistically significant changes were found in 17 sessions from 10 rats. *C*, firing suppression was observed in 10 stimulation sessions (8 rats). *D*, in the granular layer of the dentate gyrus (DG), significant increases of MUA were observed in 15 stimulation sessions from 9 rats. *E*, no significant changes were seen in 14 sessions (8 rats). *F*, firing suppression in the DG was evident in only 4 stimulation sessions from 4 rats. *G*, correlation between the magnitude of the CSD sink at the molecular layer of the DG and the corresponding change of MUA firing recorded at the granular cell layer. PSTH ratios larger than 1 indicate firing increases while PSTH ratios lower than 1 indicate firing suppression. *H*, no correlation was found between the CSD sink arriving at the stratum lacunosum moleculare (SLM) of CA1 and the MUA recorded at the stratum pyramidale of CA1. *I*, negative correlation between the CSD source recorded near the CA1 stratum pyramidale and the PSTH ratio suggest the presence of an active inhibitory process. Dashed lines represent the 95% confidence bands.

ML sink at the DG and the corresponding PSTH response at the granular layer, i.e. the stronger the sink (more negative) the more likely to detect DG firing increases (Pearson: $r = -0.67$, $P = 0.0001$; Fig. 3*G*). This suggests that somatosensory stimulation elicits a direct excitatory effect onto DG granule cells, predominantly increasing their firing in association with the current sinks that reflect excitatory dendritic inputs. Quite in contrast, distal SLM sinks appeared unable to modulate CA1 cellular firing ($r = 0.39$, $P = 0.21$; Fig. 3*H*), as previously reported for the direct temporoammonic–CA1 synapse (Leung *et al.* 1995). In addition, current sources around the CA1 cell layer negatively correlated with PSTH ratio ($r = -0.57$; $P = 0.0342$), from firing increase (PSTH > 1 for weaker SP sources) to firing suppression (PSTH < 1 for stronger SP sources, Fig. 3*I*). Such a negative correlation would not be expected if the CA1 somatic source were simply a passive return current of the SLM sink. This suggests that somatosensory stimulation elicits a complex modulatory effect onto CA1 pyramidal cells, with firing suppression depending on the strength of the somatic source giving further support to the idea that it might reflect active inhibition.

Different single-cell somatosensory responses in CA1 and DG

We further looked at cellular responses in the CA1 area and in the DG by using tetrode recordings aimed to isolate single-cell activity from 106 stimulation sessions in 13 rats. In these experiments, we mostly used stimulation of both contralateral paws due to larger stimulation artifacts when using whisker stimuli. Using semi-automatic and supervised cluster algorithms we grouped units according to amplitude variations of the waveform in different channels and standard parameters of spike width, asymmetry and firing dynamics. CA1 and DG units were classified as interneurons depending on their short trough-to-peak duration and a waveform asymmetry index (Fig. 4*A* and *B*), together with information about their spontaneous firing pattern (Fig. 5*Aa–Ea*). Cells not classified as interneurons were subsequently examined to see whether they match classification criteria for principal cells (i.e. pyramidal cells in CA1 or granule cells in the DG; see Methods).

A total of 258 units were successfully sorted (114 from CA1 and 144 from the DG) from 106 stimulation sessions. Sorted units represent a percentage of all the detected units, as multi-unit background activity was frequently activated by somatosensory stimulation. Only 17% of the sorted units in CA1 (20/114, binomial $P < 0.0001$) and about 8% in the DG (12/144, binomial $P = 0.0290$) showed statistically significant responses to peripheral stimulation, in agreement with previous reports in awake rats submitted to naturalistic stimulation (Pereira *et al.* 2007; Itskov *et al.* 2011). To quantify mean population responses we grouped responding units according to the statistical significance of the individual PSTH ratio in each stimulation session as firing suppression or firing increase (see Methods). Units from the same group (pyramidal cells, interneurons, granule cells) sharing similar statistical responses in different sessions were grouped together to estimate a mean population PSTH.

In CA1 (20 responding units), individual putative pyramidal cells (16/20) showed both firing suppression (7 sessions from 7 units, Fig. 5*Aa* and *b*) and firing increase (9 sessions from 9 units, Fig. 5*Ba* and *b*). All CA1-responding putative interneurons (4/20) exhibited a clear firing suppression pattern (6 sessions from 4 units, Fig. 5*Ca* and *b*). In contrast, in the DG (12 responding units) all putative granule cells (9/12) showed firing increases to somatosensory stimulation (9 sessions from 9 units, Fig. 5*Da* and *b*). We found three putative DG interneurons which exhibited firing increases upon somatosensory stimulation (3 sessions/3 units; Fig. 5*Ea* and *b*). While we found units responding to one stimulation site but not the other, or even switching their response type suggesting receptive field variability between cells, evidence for a somatotopic map remains unclear.

Hence, tetrode data further confirm that somatosensory stimulation activates different processes of excitation and inhibition in the CA1 and the DG of the dorsal hippocampus. While responding dentate cells and interneurons showed a consistent excitatory response, CA1 output was more elaborated with putative pyramidal cells exhibiting both firing suppression and increase after peripheral stimulation. Importantly, CA1-responding interneurons were consistently inhibited suggesting that inhibition of pyramidal cells might not be mediated locally by interneuronal circuits. However, given the large heterogeneity of hippocampal interneurons, some

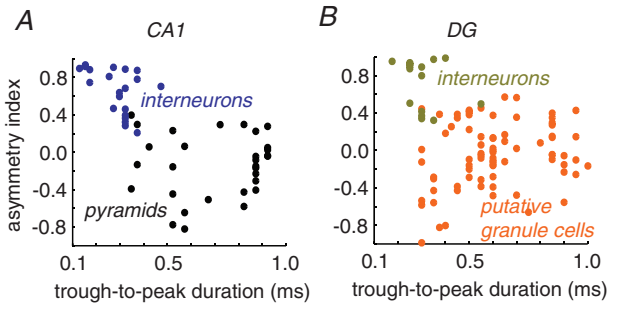

Figure 4. Unit classification from tetrode data
A, CA1 pyramidal cells and interneurons were classified from tetrode recordings using several parameters including an asymmetry index and the trough-to-peak duration of the action potential waveform. *B*, granule cells and interneurons were classified using similar criteria, together with information on firing rate modulation (theta, gamma). See Fig. 5.

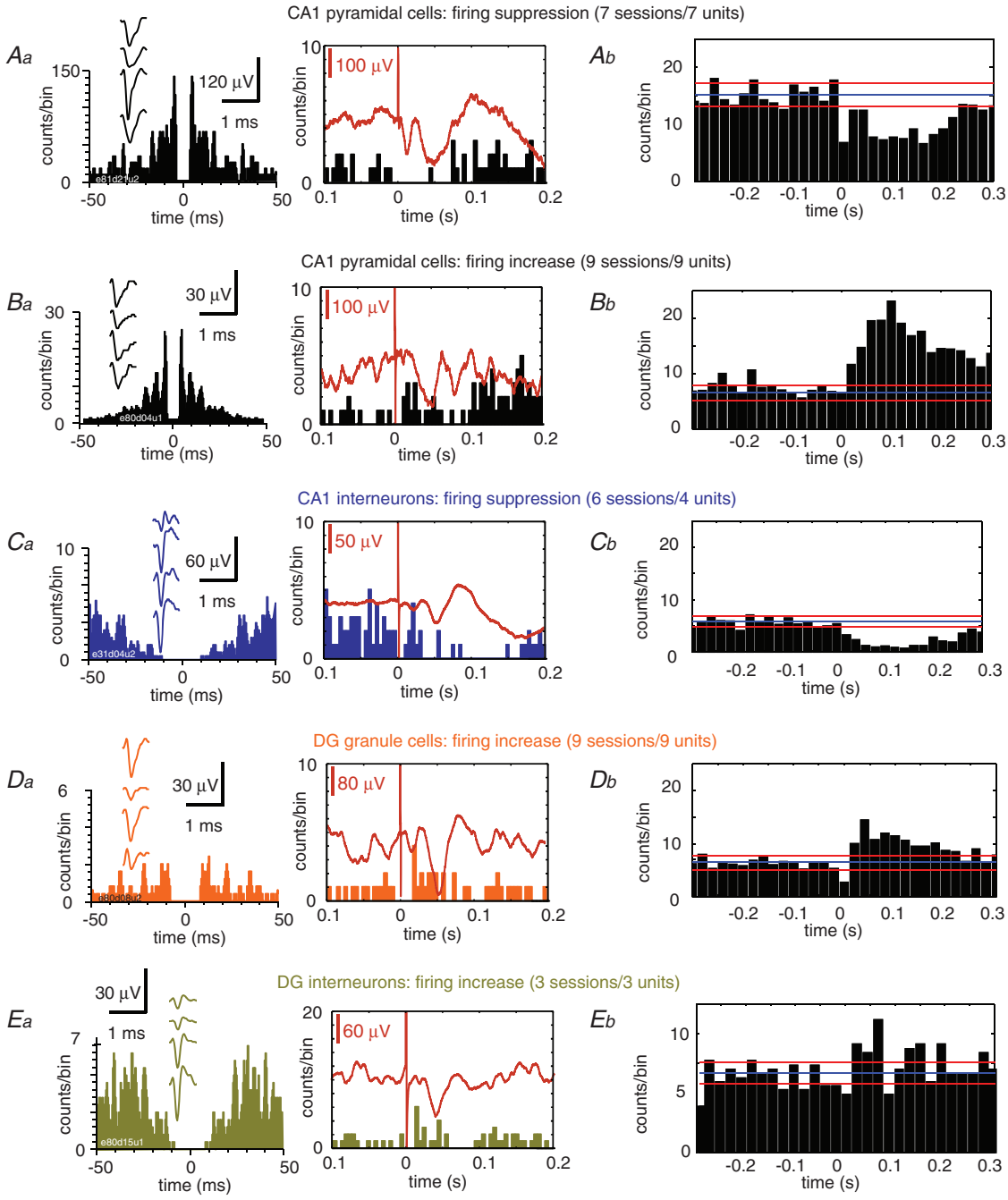

Figure 5. Unitary responses in the hippocampus to somatosensory stimulation
Data from tetrode recordings. *Aa*, example of a putative CA1 pyramidal unit exhibiting firing suppression in response to forepaw stimulation. Left panel shows the firing auto-correlogram and the mean action potential waveform from the four channels of the tetrode (insets). Right panel shows the peri-stimulus time histogram (PSTH) of the unit shown at left, together with the simultaneously recorded local field potential (red trace). *Ab*, mean PSTH data from $n = 7$ sessions from 7 putative CA1 pyramidal units exhibiting firing suppression. *Ba*, example of a putative CA1 pyramidal unit exhibiting firing increase in response to forepaw stimulation. Left panel, autocorrelogram and mean action potential waveform. Right panel, PSTH of the unit shown at left. *Bb*, mean PSTH data from $n = 9$ sessions from 9 CA1 putative pyramidal cells exhibiting firing increase. *Ca*, firing auto-correlogram (left) and PSTH (right) of a putative CA1 interneuron. *Cb*, mean PSTH from CA1 putative interneurons inhibited by somatosensory stimulation; $n = 6$ sessions from 4 units. *Da*, putative granule cells from the dentate gyrus typically exhibited excitation in response to somatosensory stimuli. Left panel: firing auto-correlogram and mean action potential waveform (inset). Right panel: PTSH of the unit shown on the left, *Db*, mean PSTH data from $n = 9$ sessions from 9 putative granule cells. *Ea*, example of firing response from a putative DG interneuron. *Eb*, mean PSTH, $n = 3$ sessions from 3 units.

of which only establish synapses onto other interneurons, these data are not conclusive regarding this cellular population. Instead, a complex inhibitory process, including interneuronal disinhibition, could be responsible for the modulation of CA1 pyramidal cell responses.

Intracellular correlates of hippocampal responses to somatosensory stimulation

We next sought for the membrane potential correlates of hippocampal responses by obtaining intracellular recordings from principal cells in CA1 and the DG of 16 rats. For proper identification of cell layer we used information from the dorsoventral coordinate and stimulated both the contralateral CA3 and the ipsilateral perforant pathway. We also applied positive and negative current pulses to monitor cell responses all along the experiment and to discriminate principal cells from interneurons based on the firing pattern and action potential attributes (see Methods, Fig. 6*Aa* and *Ba*). Due to the low probability of encountering interneurons, only data from principal cells are presented here. Similar to tetrode recordings, peripheral stimulation was mostly delivered to the hindpaw and forepaw.

We recorded a total of 22 granule cells (44 stimulation sessions) and 15 CA1 pyramidal cells (25 stimulation sessions). Somatosensory stimulation elicited statistically significant membrane potential responses in 27% of DG granule cells (6 cells in 8 sessions) and in 53% of CA1 pyramidal cells (8 cells in 9 sessions). This higher incidence of intracellular membrane potential responses as compared with tetrode data reflects the modulatory nature of somatosensory inputs over hippocampal cell firing and is in line with local field potential, CSD and MUA data.

In granule cells (6 sessions from 5 cells), responses predominantly consisted of an early (onset 51 ± 25 ms; peak 84 ± 45 ms) mild mean depolarization of 0.86 ± 0.44 mV (Fig. 6*Ab*). The large mean latency in the intracellular peak, as compared with CSD peak latencies, is likely to reflect variability of the small sample of cells. The dynamics of somatodendritic propagation could also account for latency difference between these two signals. In one granule cell, we found hyperpolarizing responses to both hindpaw and forepaw stimulation. In those granule cells examined across sessions there was consistence of response type ($n = 4$ cells). These data give additional support to a major excitatory drive of somatosensory stimulation over dentate granule cells, in agreement with CSD, MUA and tetrode observations.

In the majority of responding CA1 pyramidal cells (6 sessions from 5 cells), we found hyperpolarized potentials (-0.99 ± 0.64 mV) that peaked at 107 ± 44 ms (onset 61 ± 29 ms) after stimulation (Fig. 6*Bb*). This confirms the active inhibitory nature of the current source detected around the CA1 cell layer after somatosensory stimulation. Consistent with tetrode data, in three cells (3 sessions), we found a depolarizing response of 0.83 ± 0.78 mV that peaked at 61 ± 23 ms (onset 34 ± 17 ms) and mediated neuronal firing (Fig. 6*Bc*).

Therefore, intracellular recordings revealed different membrane potential responses of DG and CA1 to somatosensory stimulation that clarify their firing behaviour. Such different dynamics suggest that somatosensory signals initiate different processes of excitation and inhibition in the input and output regions of the hippocampus. Altogether, CSD, MUA, tetrode and intracellular data suggest that differences in the strength and composition of synaptic inputs, regulated by a different balance of excitation and inhibition, is responsible for the variability and richness of hippocampal somatosensory responses.

State dependence of somatosensory-evoked hippocampal responses

Previous work in freely moving animals suggests that hippocampal responses to sensory stimulation depend on the state of ongoing hippocampal oscillations (Brankack & Buzsaki, 1986; Pereira *et al.* 2007), which is organized in episodes of theta rhythm, slow oscillations (<1 Hz) and large irregular activities (LIA). In the urethane preparation, brain activity spontaneously fluctuates between different oscillatory states, similarly to natural sleep (Clement *et al.* 2008). We therefore wondered about the influence of brain state on the hippocampal response to somatosensory stimulation.

To evaluate state-dependent changes of hippocampal responses, we looked at local field potential dynamics in the seconds preceding individual stimuli. Hippocampal state was classified as theta (Fig. 7*Aa*) or non-theta (slow oscillations + LIA; Fig. 7*Ab*) according to the main oscillatory frequency on a trial-by-trial basis. We examined 16 stimulation sessions from nine rats that showed a sufficient number of transitions between theta and non-theta states for statistical purposes. In agreement with results in freely moving animals, hippocampal responses were smaller during theta than during non-theta states in the urethane-anaesthetized preparation (Fig. 7*Ba versus Bb*). Response difference reached significance at the ML of the DG both for local field potentials (Fig. 7*C*) and CSD (Fig. 7*D*). Therefore, part of the variability in the strength of the ML sink described before (Fig. 3*G*) could be attributed to state-dependent fluctuations of the hippocampal state.

Cortical modulation of hippocampal responses to somatosensory stimulation

In awake rats, the 'local' state of hippocampal oscillatory activity depends on the behavioural state of the animal (Winson & Abzug, 1978*b*) and consequently correlates with the 'distant' state of cortical oscillatory activity (Gervasoni *et al.* 2004; Wolansky *et al.* 2006). The theta/non-theta state-dependent changes previously described in hippocampal somatosensory responses could also reflect, at least in part, changes of cortical somatosensory responses. In order to further understand the influence of cortical activity on hippocampal responses we performed a combined spectral analysis

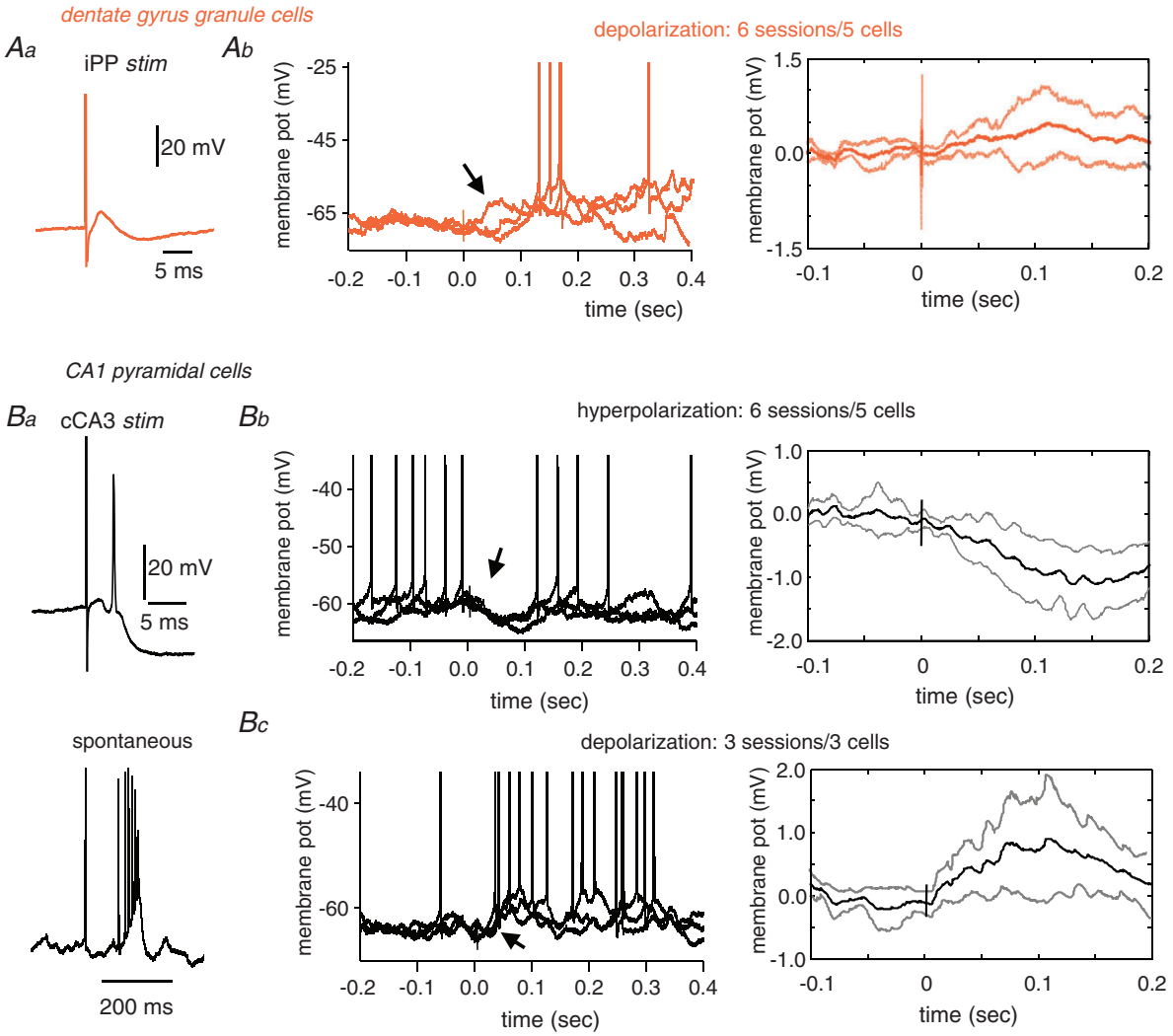

Figure 6. Intracellular responses to somatosensory stimulation
Aa, granule cells intracellularly recorded in the dentate gyrus were tested with stimulation of the ipsilateral perforant pathway (iPP). *Ab*, left, example of three individual traces of a representative granule cell showing depolarizing responses to somatosensory stimulation (hindpaw). Spikes are truncated to highlight changes of membrane potentials. Arrow points to the early membrane depolarizing response. *Ab*, right, grand average of the mean membrane potential response from $n = 6$ sessions from 5 granule cells showing depolarizing responses. *Ba*, CA1 pyramidal cells were characterized by their response to the stimulation of the contralateral CA3 (cCA3) (upper panel) and their typical spontaneous firing pattern consisting of complex-spike bursts (lower panel). *Bb*, left, example of three individual traces of a typical CA1 pyramidal cell showing hyperpolarizing responses to hindpaw stimulation. Spikes are truncated. Note membrane potential hyperpolarization resulting in firing suppression (arrow). *Bb*, right, grand average of the mean membrane potential response from $n = 6$ sessions from 5 CA1 pyramidal cells. *Bc*, left, example of three individual traces of the intracellular response of the complex-spike cell shown at B1 that responded with depolarization to hindpaw stimulation. Spikes are truncated to highlight membrane changes (arrow). *Bc*, right, grand average of the mean membrane potential response from $n = 3$ sessions from 3 CA1 pyramidal cells that exhibited depolarizing responses.

of both the cortical and the hippocampal signals. To this purpose we performed a new set of experiments (46 stimulation sessions from 10 rats) with continuous simultaneous hippocampal (DG) and cortical recordings (primary somatosensory cortex) to look for the state dynamics between these areas (Fig. 8*A*). The cortical state was classified as slow-wave (SW) or activated based on the integral of the power spectrum (Fig. 8*B*, upper graph). The hippocampal state was classified as theta or non-theta based on the peak frequency of the power spectrum (Fig. 8*B*, lower graph).

Plotting together these indices, we investigated the joint state dynamics of the hippocampus and the primary somatosensory cortex in 18 stimulation sessions from seven rats with sufficient SW-activated state transitions. Data typically formed clusters reflecting the correspondence between cortical and hippocampal states as a feature of global brain dynamics (Fig. 8*C*). Hippocampal non-theta states were typically associated with cortical SW activity, while theta activity in the hippocampus tended to occur in association with an activated cortical state. Disturbances to this organization occurred during transitions (Fig. 8*A*, arrows). Consistent with results above on theta modulation, hippocampal responses to somatosensory stimuli during cortical SW activity were significantly larger than those occurring during the activated cortical state (Fig. 8*D*).

We next investigated the relationship between the phase of cortical up and down states during slow-wave activity and the hippocampal response to somatosensory stimulation in rats with sufficient numbers of up–down transitions (23 stimulation sessions from 9 rats). As expected from the literature (Sachdev *et al.* 2004; Hasenstaub *et al.* 2007; Aguilar *et al.* 2010), cortical somatosensory responses were significantly larger if stimulation occurred during the down rather than during

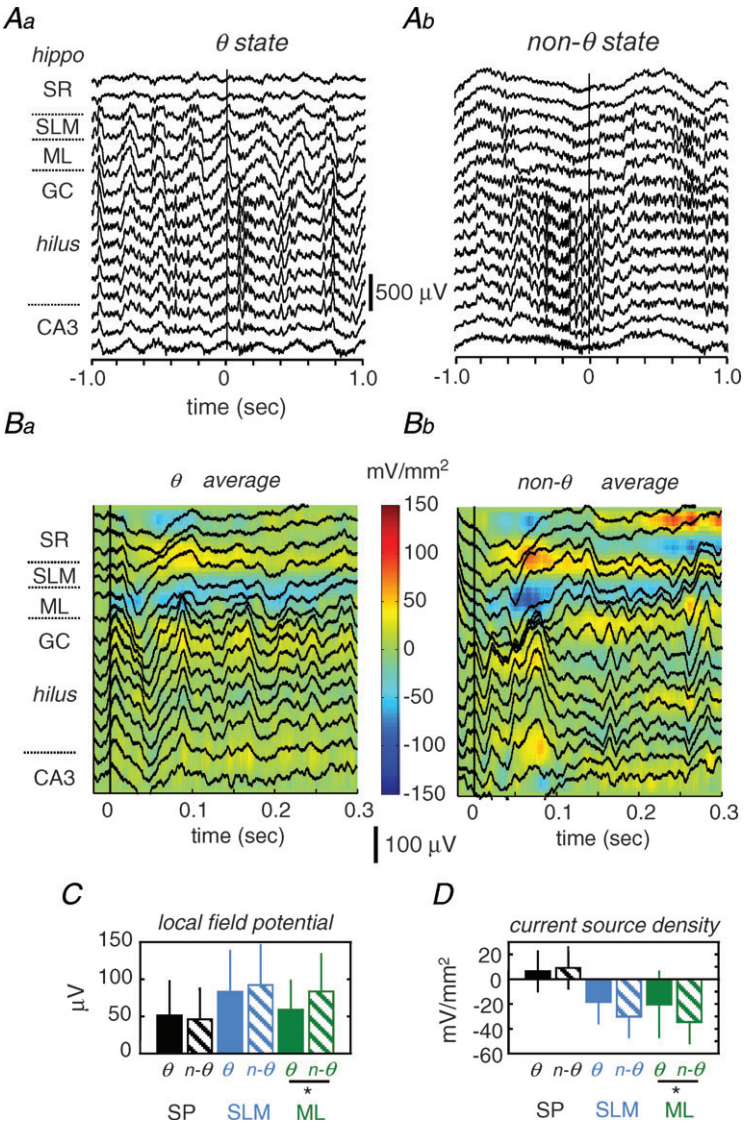

Figure 7. Influence of the hippocampal state on responses to somatosensory stimulation
A, the hippocampal state just preceding individual stimuli was classified as theta (*θ*, *Aa*) or non- theta (*Ab*) according to spectral information. *B*, individual stimuli applied during theta (*Ba*) and non-theta (*Bb*) states were averaged to calculate mean local field potential responses and current source density (CSD) maps. *C*, mean local field potentials from the molecular layer (ML) of the dentate gyrus were significantly smaller during theta *versus* non-theta states (*paired *t* test: $P = 0.0462$). *D*, CSD responses from the ML were significantly smaller during theta *versus* non-theta states (*$P < 0.0351$). SP, stratum pyramidale; SLM, stratum lacunosum moleculare.

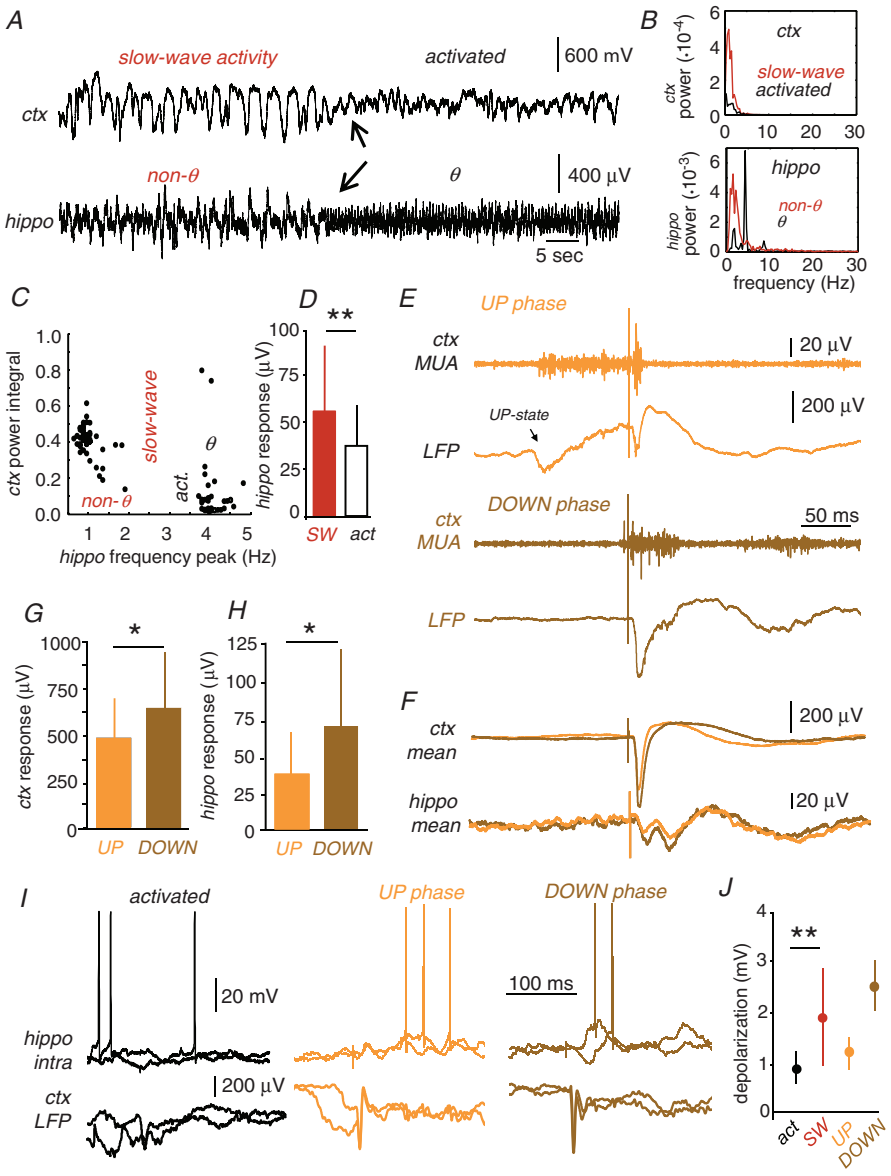

Figure 8. Cortical modulation of hippocampal responses to somatosensory stimulation
A, simultaneous recordings of hippocampal (granular layer of the dentate gyrus) and cortical (primary somatosensory cortex) activity permitted us to investigate the joint state dynamics and their influence in hippocampal responses. Cortical states were classified as slow-wave activity or activated state. The hippocampal state was classified as theta or non-theta. Arrows point to the state transition in both the cortex and the hippocampus. *B*, power spectral analysis of the cortical and hippocampal signals shown in *A* during the different states. *C*, example of the joint state dynamics of hippocampal and cortical activity. Clusters of similar dynamical states were typically formed. *D*, hippocampal local field potential (LFP) responses obtained during episodes of cortical slow-wave activity (SW) were significantly larger than those obtained during the activated state (**paired *t* test, $P = 0.0060$). *E*, individual somatosensory stimuli can arrive at different phases of slow-wave activity. Stimuli can either arrive during a cortical up state (UP phase, orange) or during a down state (DOWN phase, brown). *F*, both the cortical and the hippocampal response were smaller for those stimuli arriving during the UP than during the DOWN phase. *G*, LFP cortical averaged response was smaller when the stimuli occurred during the UP compared to DOWN phases of SW activity (**paired *t* test: $P < 0.0001$). *H*, the LFP hippocampal averaged response was smaller during UP compared to DOWN phases of cortical SW activity (*paired *t* test: $P = 0.0195$). *I*, intracellular responses recorded in a representative granule cell during the activated (black) and the UP (orange) and DOWN (brown) phases of cortical slow-wave activity. LFP activity in the primary somatosensory cortex was recorded simultaneously. *J*, mean depolarizing responses recorded in granule cells as a function of the distant cortical state grouped as activated (act., black) and slow-wave (SW, red). Data from 6 sessions from 4 cells. **$P = 0.0079$. Dependence of mean depolarizing responses with the UP–DOWN phase is also shown. Data from 2 sessions from 2 granule cells.

the up phase of SW oscillations (Fig. 8*E* and *G*). We found that hippocampal somatosensory responses displayed a similar dependence on the phase of the cortical up–down state (Fig. 8*F* and *H*), suggesting that the classical state-dependent modulation of evoked responses in the primary somatosensory cortex is reflected in the hippocampus.

Finally, we recorded intracellularly from dentate granule cells while simultaneously monitoring the primary somatosensory cortex (23 stimulation sessions in 18 granule cells from 8 rats). We found statistical responses in six sessions from four granule cells that we further examined to look for response differences depending on the phase of activity in the corresponding primary somatosensory cortex. In agreement with local field potential data, the intracellular depolarizing response of granule cells was smaller when the primary somatosensory cortex was in an activated state *versus* SW activity (Fig. 8*I* and *J*). In two sessions from two cells we had sufficient phase fluctuations between the up and down phases of SW activity to further examine cycle differences within the cell. The intracellular depolarizing response was larger for stimuli occurring in the down than in the up phase of cortical activity (Fig. 8*I* and *J*). These data suggest that in addition to a 'local' state-dependence, somatosensory-evoked hippocampal responses are also modulated by the phase of 'distant' slow-wave cortical oscillations.

Discussion

Our data reveal the nature of the elementary responses of the hippocampus to incoming somatosensory inputs. Somatosensory inputs consistently reached the hippocampus at the ML, through the perforant pathway originating in layer II entorhinal cortex to discharge dentate granule cells. While a similar input to CA1 could be less consistently detected at the SLM via the temporoammonic pathway, the firing rate of CA1 pyramidal cells was found to be under strong inhibitory control. Importantly, a delayed current source at the CA1 pyramidal cell layer corresponded to membrane potential hyperpolarization recorded intracellularly, confirming the inhibitory response of CA1 cells. Such a different somatosensory-evoked response in DG and CA1 might be reflecting distinct functional organization of extra-hippocampal inputs to these hippocampal areas. This different contribution of excitation and inhibition at CA1 and DG, together with state-dependent fluctuations in the strength of synaptic inputs, are critical to understand the richness of somatosensory-evoked responses in the hippocampus.

Early evoked-potential studies suggested that the hippocampus could be involved in processing sensory information of different modalities both in humans (Wilson *et al.* 1984) and experimental animals (Miller & Groves, 1977; Deawyler *et al.* 1981; Brankack & Buzsaki, 1986; Canning *et al.* 2000; Vinogradova, 2001). One common result to most of these studies was that hippocampal responses were similar for different modalities, so that the different sensory channels might share common pathways once they reach the entorhinal cortex. According to our data, an initial current sink (about 35–40 ms) reaches the hippocampus at the ML of the DG, sometimes accompanied by a sink at the SLM of CA1. The DG sink is mirrored by a source in the granular cell layer of the DG that reflects the sensory-evoked depolarization of granule cells, as confirmed by our multi-unit, tetrode and intracellular recordings. Anatomical data suggest that parallel inputs run from the perirhinal and postrhinal cortices to the entorhinal region to activate different pathways to the hippocampus (Witter *et al.* 2000). One circuit will directly loop the entorhinal and the tri-synaptic hippocampal circuits via the perforant pathway (Witter *et al.* 2000), being responsible for the observed activation of dentate granule cells. The second parallel temporoammonic pathway runs from layer III of the entorhinal cortex directly into the CA1/subiculum (Witter *et al.* 2000), possibly underlying the SLM sinks. Interestingly, the SLM CA1 sink appeared to be independent from the DG sink, not being consistently present in all sessions. In CA1, the SLM sink is often shortly followed (40–45 ms) by an outlasting current source near the CA1 pyramidal cell layer. Both current signals are not precisely counterbalanced, suggesting that the source would be associated with an active flow of negative charges flowing into CA1 pyramidal cells. We confirmed the inhibitory nature of the CA1 response both in multi-unit, tetrode and intracellular recordings. Nevertheless, the fact that a proportion of CA1 pyramidal cells were found to fire at latencies similar to the associated distal dendritic current sink might suggest that sensory information could directly reach CA1. However, given the absence of clear Schaffer activation (Fig. 1*Da*) and the poor firing modulation exerted by distal SLM sinks (Fig. 3*H*; Leung *et al.* 1995), this excitatory response is more likely to reflect some modulatory process potentially mediated by firing suppression in interneurons (Fig. 5*Ca*). Thus, our data reveal that CA1 neuronal firing is dominated by the level of inhibition suggesting somatosensory stimulation elicits a complex modulatory effect onto this region (Witter *et al.* 2000; Ang *et al.* 2005).

What is the nature of the inhibitory response in CA1 pyramidal cells? Previous work noted early voltage positivity in the pyramidal cell layer of CA1 in response to both acoustic and tooth pulp stimulation (Brankack & Buzsaki, 1986). Similar to our data in the anaesthetized rat, the typical CA1 response in freely moving animals was firing suppression, which was thought to be mediated by

the action of interneurons activated by subcortical inputs (Brankack & Buzsaki, 1986; Vinogradova, 2001). With our tetrode recordings, all CA1-sorted interneurons showed either no response or a clear suppression of their firing rate, suggesting that the inhibitory response detected in pyramidal cells might not be mediated by local interneurons. One possibility is that hippocampal responding interneurons are located far from the stratum pyramidale, not being targeted by our tetrode recordings (Brankack & Buzsaki, 1986). Another possibility is a disinhibitory effect mediated by some interneuronal population driven by interneuron-specific cells (Gulyas *et al.* 1996). Interestingly, entorhinal projecting GABAergic interneurons have been described to specifically target hippocampal interneurons in the SLM/SR border (Germroth *et al.* 1989; Melzer *et al.* 2012). Alternatively, subcortical inhibitory projections could participate (Herreras *et al.* 1988*b*). Indeed, neurons in the septum discharge in response to multimodal sensory stimulation, as revealed by single-unit recordings (Vinogradova, 1993, 2001). Interestingly, septal transection resulted in elimination of the typical hippocampal firing suppression (Miller & Groves, 1977).

We found no clear evidence for activation of Schaffer collaterals after somatosensory stimulation, i.e. no sink was typically detected at the stratum radiatum of CA1, in contrast to previous suggestions based on laminar voltage recordings but not on CSD signals (Brankack & Buzsaki, 1986). Our data are rather in agreement with results from single-cell recordings showing a progressive inhibition of CA3 neuronal firing after repetitive sensory stimulation (Vinogradova, 2001; Villarreal *et al.* 2007). Such CA3 firing rate suppression might be determined by disynaptic inhibition driven by responding granule cells (Brankack & Buzsaki, 1986; Vinogradova, 2001). The absence of Schaffer activation could be then linked with DG activation as a mechanism for releasing the CA1 region from intra-hippocampal control.

Previous anatomical and electrophysiological data suggest an important role of the reuniens nucleus of the thalamus in the modulation of hippocampal activity (Dolleman *et al.* 1997; Bertram & Zhang, 1999). Given the known laminar distribution of these terminals at the SLM of the CA1 region (Wouterlood *et al.* 1990), it might be argued that part of the responses described here are more likely to reflect thalamic activation rather than entorhinal cortical inputs. However, anatomical data suggest that somatosensory inputs from the lemniscus to the reuniens are sparse and weak (Krout *et al.* 2002). Instead, midline thalamic nuclei are more likely to be involved in neuromodulatory action served by inputs from brainstem structures, including the locus coeruleus, ventral tegmental area, superior colliculus and the entire raphe (Van der Werf *et al.* 2002).

We found that variability was a major characteristic of neuronal responses to somatosensory stimuli recorded at the hippocampus, a distant brain region in the propagation pathway of incoming somatosensory information. This fits well with the idea that the increase in response variability and sparseness from the periphery to brain areas supporting higher levels of sensory processing could promote efficient coding distributed in large populations of neurons (Olshausen & Field, 2004; Scaglione *et al.* 2011). Early studies already reflected such a feature in recordings of neuronal firing. Miller & Groves (1977) examined neuronal responses in different hippocampal regions to visual, auditory and tactile stimulation. They found that up to 60% of responding neurons exhibited excitatory responses consistent of firing increases, a relatively high percentage of cells (35%) exhibited firing suppression, and a small group of cells (6%) showed both excitation and inhibition of their baseline firing rate. Branckak & Buzsaki (1986) tried to understand this variability by relating neuronal location within the hippocampus, time of stimulus presentation and the behavioural response of the animal. They reported typical firing suppression in CA1 putative pyramidal cells, sometimes followed by firing increases, and mostly excitatory responses of putative granule cells, which were strongly modulated by the animal behaviour following stimulus presentation. Later on, Vinogradova and colleagues analysed single-cell responses in identified hippocampal regions upon different types of peripheral stimulus (Vinogradova *et al.* 1993, 2001). In the dentate gyrus, cellular responses were consistently associated with variable tonic and phasic firing (Vinogradova *et al.* 1993). In the CA1 region, from a total of 68% responding neurons, the great majority exhibited firing rate suppression, whereas firing increase was observed in about 40% (Vinogradova, 2001).

According to our MUA, tetrode and intracellular data, this richness of the hippocampal response could be partly attributable to differences in the strength and composition of synaptic inputs. Here, we provide for the first time converging local field potential, multi-unit, tetrode and intracellular data to understand the basic properties of these hippocampal responses and to interpret the multiple sources of variability, including spatial location within the hippocampus, stimulus location on the body and the state and the phase of brain oscillations. We found that both the local (hippocampal) and the distant (cortical) state of ongoing oscillatory activity strongly modulate the overall response to stimulation, being smaller when the cortex is in its activated state and the hippocampus exhibits theta activity. This is in close agreement with the effect reported in the hippocampus of freely moving animals showing a smaller somatosensory-related response during theta-related behaviours (Brankack & Buzsaki, 1986; Pereira *et al.* 2007). Internal hippocampal processing is

also dominated by the state, with different modulatory action in the perforant pathway and the hippocampal associational pathways (Winson & Abzug, 1978*a*; Herreras *et al.* 1988*a*). While brain dynamics have a global influence on neuronal responses (Contreras & Steriade, 1997; Vinogradova, 2001; Gervasoni *et al.* 2004; Sachdev *et al.* 2004; Sakata & Harris, 2009, but see Stoelzel *et al.* 2009), we found that the phase of the cortical activation can further interfere with hippocampal processing. According to our data, sensory inputs occurring during active cortical phases would compete with the invasion of these active cortical phases running in parallel through the same input pathway to the hippocampus (Isomura *et al.* 2006; Hahn *et al.* 2007). Other factors like the level of arousal and attention are known to modulate hippocampal excitability (Leung, 1980; Vinogradova, 2001; Tai *et al.* 2012) pointing to a complex interaction between the ongoing oscillations and the arrival of sensory information. Therefore, the hippocampal response is considerably modulated by cortical and subcortical structures during theta-related behaviour, such as walking, rearing and sniffing, suggesting that convergent streams of information participate in creating an integrated neuronal representation.

References

Aguilar J, Humanes-Valera D, Alonso-Calviño E, Yague JG, Moxon KA, Oliviero A & Foffani G (2010). Spinal cord injury immediately changes the state of the brain. *J Neurosci* **30**, 7528–7537.

Ang CW, Carlson GC & Coulter DA (2005). Hippocampal CA1 circuitry dynamically gates direct cortical inputs preferentially at theta frequencies. *J Neurosci* **25**, 9567–9580.

Bertram EH & Zhang DX (1999). Thalamic excitation of hippocampal CA1 neurons: a comparison with the effects of CA3 stimulation. *Neuroscience* **92**, 15–26.

Brankack J & Buzsáki G (1986). Hippocampal responses evoked by tooth pulp and acoustic stimulation: depth profiles and effect of behaviour. *Brain Res* **378**, 303–314.

Burwell RD & Amaral DG (1998). Cortical afferents of the perirhinal, postrhinal, and entorhinal cortices of the rat. *J Comp Neurol* **398**, 179–205.

Canning KJ, Wu K, Peloquin P, Kloosterman F & Leung LS (2000). Physiology of the entorhinal and perirhinal projections to the hippocampus studied by current source density analysis. *Ann N Y Acad Sci* **911**, 55–72.

Clement EA, Richard A, Thwaites M, Ailon J, Peters S & Dickson CT (2008). Cyclic and sleep-like spontaneous alternations of brain state under urethane anaesthesia. *PloS One* **3**, e2004.

Contreras D & Steriade M (1997). State-dependent fluctuations of low-frequency rhythms in corticothalamic networks. *Neuroscience* **76**, 25–38.

Csicsvari J, Hirase H, Czurkó A, Mamiya A & Buzsáki G (1999). Oscillatory coupling of hippocampal pyramidal cells and interneurons in the behaving rat. *J Neurosci* **19**, 274–287.

Deadwyler SA, West MO & Robinson JH (1981). Evoked potentials from the dentate gyrus during auditory stimulus generalization in the rat. *Exp Neurol* **71**, 615–624.

Dolleman-Van der Weel MJ, Lopes da Silva FH & Witter MP (1997). Nucleus reuniens thalami modulates activity in hippocampal field CA1 through excitatory and inhibitory mechanisms. *J Neurosci* **17**, 5640–5650.

Eacott MJ & Norman G (2004). Integrated memory for object, place, and context in rats: a possible model of episodic-like memory? *J Neurosci* **24**, 1948–1953.

Eichenbaum H (2004). Hippocampus: cognitive processes and neural representations that underlie declarative memory. *Neuron* **44**, 109–120.

Freeman JA & Nicholson C (1975). Experimental optimization of current source-density technique for anuran cerebellum. *J Neurophysiol* **38**, 369–382.

Friedberg MH, Lee SM & Ebner FF (1999). Modulation of receptive field properties of thalamic somatosensory neurons by the depth of anaesthesia. *J Neurophysiol* **81**, 2243–2252.

Germroth P, Schwerdtfeger WK & Buhl EH (1989). GABAergic neurons in the entorhinal cortex project to the hippocampus. *Brain Res* **494**, 187–192.

Gervasoni D, Lin S-C, Ribeiro S, Soares ES, Pantoja J & Nicolelis MAL (2004). Global forebrain dynamics predict rat behavioral states and their transitions. *J Neurosci* **24**, 11137–11147.

Gulyas AI, Hajos N & Freund TF (1996). Interneurons containing calretinin are specialized to control other interneurons in the rat hippocampus. *J Neurosci* **16**, 3397–3411.

Hahn TTG, Sakmann B & Mehta MR (2007). Differential responses of hippocampal subfields to cortical up-down states. *Proc Natl Acad Sci U S A* **104**, 5169–5174.

Hasenstaub A, Sachdev RNS & McCormick DA (2007). State changes rapidly modulate cortical neuronal responsiveness. *J Neurosci* **27**, 9607–9622.

Herreras O, Solís JM, Herranz AS, Martín del Río R & Lerma J (1988*a*). Sensory modulation of hippocampal transmission. II. Evidence for a cholinergic locus of inhibition in the Schaffer-CA1 synapse. *Brain Res* **461**, 303–313.

Herreras O, Solís JM, Muñoz MD, Martín del Río R & Lerma J (1988*b*). Sensory modulation of hippocampal transmission. I. Opposite effects on CA1 and dentate gyrus synapsis. *Brain Res* **461**, 290–302.

Hill DN, Mehta SB & Kleinfeld D (2011). Quality metrics to accompany spike sorting of extracellular signals. *J Neurosci* **31**, 8699–8705.

Ibarz JM, Foffani G, Cid E, Inostroza M & Menendez de la Prida L (2010). Emergent dynamics of fast ripples in the epileptic hippocampus. *J Neurosci* **30**, 16249–16261.

Isomura Y, Sirota A, Ozen S, Montgomery S, Mizuseki K, Henze DA & Buzsáki G (2006). Integration and segregation of activity in entorhinal-hippocampal subregions by neocortical slow oscillations. *Neuron* **52**, 871–882.

Itskov PM, Vinnik E & Diamond ME (2011). Hippocampal representation of touch-guided behaviour in rats: persistent and independent traces of stimulus and reward location. *PloS One* **6**, e16462.

Khanna S & Sinclair JG (1992). Responses in the CA1 region of the rat hippocampus to a noxious stimulus. *Exp Neurol* **117**, 28–35.

Krout KE, Belzer RE & Loewy AD (2002). Brainstem projections to midline and intralaminar thalamic nuclei of the rat. *J Comp Neurol* **448**, 53–101.

Leung LS (1980). Behavior-dependent evoked potentials in the hippocampal CA1 region of the rat. I. Correlation with behaviour and EEG. *Brain Res* **198**, 95–117.

Leung LS, Roth L & Canning KJ (1995). Entorhinal inputs to hippocampal CA1 and dentate gyrus in the rat: a current-source-density study. *J Neurophysiol* **73**, 2392–2403.

Lilja J, Endo T, Hofstetter C, Westman E, Young J, Olson L & Spenger C (2006). Blood oxygenation level-dependent visualization of synaptic relay stations of sensory pathways along the neuroaxis in response to graded sensory stimulation of a limb. *J Neurosci* **26**, 6330–6336.

Makarov V, Makarova J & Herreras O (2010). Disentanglement of local field potential sources by independent component analysis. *J Comp Neurosci* **29**, 445–457.

Melzer S, Michael M, Caputi A, Eliava M, Fuchs EC, Whittington MA & Monyer H (2012). Long-range-projecting GABAergic neurons modulate inhibition in hippocampus and entorhinal cortex. *Science* **335**, 1506–1510.

Miller SW & Groves PM (1977). Sensory evoked neuronal activity in the hippocampus before and after lesions of the medial septal nuclei. *Physiol Behav* **18**, 141–146.

O'Keefe J & Nadel L (1978). *The Hippocampus as a Cognitive Map*. Oxford University Press.

Olshausen BA & Field DJ (2004). Sparse coding of sensory inputs. *Curr Opin Neurobiol* **14**, 481–487.

Pereira A, Ribeiro S, Wiest M, Moore LC, Pantoja J, Lin S-C & Nicolelis MAL (2007). Processing of tactile information by the hippocampus. *Proc Natl Acad Sci U S A* **104**, 18286–18291.

Ranck JB (1973). Studies on single neurons in dorsal hippocampal formation and septum in unrestrained rats. I. Behavioral correlates and firing repertoires. *Exp Neurol* **41**, 461–531.

Sachdev RNS, Ebner FF & Wilson CJ (2004). Effect of subthreshold up and down states on the whisker-evoked response in somatosensory cortex. *J Neurophysiol* **92**, 3511–3521.

Sainsbury RS, Heynen A & Montoya CP (1987). Behavioral correlates of hippocampal type 2 theta in the rat. *Physiol Behav* **39**, 513–519.

Sakata S & Harris KD (2009). Laminar structure of spontaneous and sensory-evoked population activity in auditory cortex. *Neuron* **64**, 404–418.

Scaglione A, Moxon KA, Aguilar J & Foffani G (2011). Trial-to-trial variability in the responses of neurons carries information about stimulus location in the rat whisker thalamus. *Proc Natl Acad Sci U S A* **108**, 14956–14961.

Sirota A, Montgomery S, Fujisawa S, Isomura Y, Zugaro M & Buzsáki G (2008). Entrainment of neocortical neurons and gamma oscillations by the hippocampal theta rhythm. *Neuron* **60**, 683–697.

Smith PF (1997). Vestibular-hippocampal interactions. *Hippocampus* **7**, 465–471.

Stoelzel CR, Bereshpolova Y & Swadlow HA (2009). Stability of thalamocortical synaptic transmission across awake brain states. *J Neurosci* **29**, 6851–6859.

Tai SK, Ma J, Ossenkopp KP & Leung LS (2012). Activation of immobility-related hippocampal theta by cholinergic septohippocampal neurons during vestibular stimulation. *Hippocampus* **22**, 914–925.

Van der Werf YD, Witter MP & Groenewegen HJ (2002). The intralaminar and midline nuclei of the thalamus. Anatomical and functional evidence for participation in processes of arousal and awareness. *Brain Res Brain Res Rev* **39**, 107–140.

Villarreal DM, Gross AL & Derrick BE (2007). Modulation of CA3 afferent inputs by novelty and theta rhythm. *J Neurosci* **27**, 13457–13467.

Vinogradova OS (2001). Hippocampus as comparator: role of the two input and two output systems of the hippocampus in selection and registration of information. *Hippocampus* **11**, 578–598.

Vinogradova OS, Brazhnik ES, Kitchigina VF & Stafekhina VS (1993). Acetylcholine, theta-rhythm and activity of hippocampal neurons in the rabbit–IV. Sensory stimulation. *Neuroscience* **53**, 993–1007.

Wilson CL, Babb TL, Halgren E, Wang ML & Crandall PH (1984). Habituation of human limbic neuronal response to sensory stimulation. *Exp Neurol* **84**, 74–97.

Winson J & Abzug C (1978*a*). Dependence upon behaviour of neuronal transmission from perforant pathway through entorhinal cortex. *Brain Res* **147**, 422–427.

Winson J & Abzug C (1978*b*). Neuronal transmission through hippocampal pathways dependent on behaviour. *J Neurophysiol* **41**, 716–732.

Witter MP (2007). The perforant path: projections from the entorhinal cortex to the dentate gyrus. *Prog Brain Res* **163**, 43–61.

Witter MP, Naber PA, van Haeften T, Machielsen WC, Rombouts SA, Barkhof F, Scheltens P & Lopes da Silva FH (2000). Cortico-hippocampal communication by way of parallel parahippocampal-subicular pathways. *Hippocampus* **10**, 398–410.

Wolansky T, Clement EA, Peters SR, Palczak MA & Dickson CT (2006). Hippocampal slow oscillation: a novel EEG state and its coordination with ongoing neocortical activity. *J Neurosci* **26**, 6213–6229.

Wouterlood FG, Saldana E & Witter MP (1990). Projection from the nucleus reuniens thalami to the hippocampal region: light and electron microscopic tracing study in the rat with the anterograde tracer *Phaseolus vulgaris*-leucoagglutinin. *J Comp Neurol* **296**, 179–203.

Yague JG, Foffani G & Aguilar J (2011). Cortical hyperexcitability in response to preserved spinothalamic inputs immediately after spinal cord hemisection. *Exp Neurol* **227**, 252–263.

Author contributions

G.F., J.A. and L.M.P. designed the study. E.B. performed multi-channel and tetrode experiments and together with J.A.

obtained and analysed intracellular data. J.R.B.-M. and L.M.P. performed cell sorting. E.B., G.F. and L.M.P. were responsible for data analysis and together wrote the paper. All authors approved the final version of the manuscript.

Acknowledgements

This work was supported by grants from the Spanish Ministry Ministerio de Ciencia e Innovación (MICINN) (BFU2009-07989) to L.M.P. and from La Fundación para la Investigación Sanitaria en Castilla la Mancha (PI-2006/49), Gobierno de Castilla-La Mancha, to L.M.P. and G.F. E.B. was supported by a PhD fellowship from Fundación para la Investigación Sanitaria en Castilla la Mancha (MOV-2010_JI/004). We thank Elena Cid for helping us with histological localization and Miguel Maravall, Xavier Leinekugel and the Charpier Lab for useful comments and suggestions.